NASA Technical Memorandum 100286

Compensation of Reflector Antenna Surface Distortion Using an Array Feed

A.R. Cherrette
University of Illinois
Urbana, Illinois

R.J. Acosta
Lewis Research Center
Cleveland, Ohio

P.T. Lam
Lockheed Missiles and Space Company
Sunnyvale, California

and

S.W. Lee
University of Illinois
Urbana, Illinois

January 1988

NASA

COMPENSATION OF REFLECTOR ANTENNA SURFACE DISTORTION USING AN ARRAY FEED*

A.R. Cherrette
University of Illinois
Dept. of Electrical and Computer Engineering
Urbana, Illinois 61801

R.J. Acosta
National Aeronautics and Space Administration
Lewis Research Center
Cleveland, Ohio 44135

P.T. Lam
Lockheed Missiles and Space Company
Sunnyvale, California 94088

and

S.W. Lee
University of Illinois
Dept. of Electrical and Computer Engineering
Urbana, Illinois 61801

SUMMARY

The dimensional stability of the surface of a large reflector antenna is important when high gain/low sidelobe performance is desired. If the surface is distorted due to thermal or structural reasons, antenna performance can be improved through the use of an array feed. The design of the array feed and its relation to the surface distortion are examined in this paper. The sensitivity of antenna performance to changing surface parameters for fixed feed array geometries is also studied. This allows determination of the limits of usefulness for feed array compensation.

*Work performed under NASA Grant NAG3-419.

1. Introduction and Overview

Maintaining the surface accuracy of a large reflector antenna is important when high gain/low sidelobe performance is desired. Reflectors surface errors are generally classified into two following types:

(i) The random surface error in the order of several mils due to manufacture imperfection [1-3].

(ii) The large-scaled surface error in the order of inches due to structural or thermal causes [4] [5].

It is the large-scaled surface error that is of interest here. Methods for reducing this error include the use of better antenna supporting structures, better thermal-insensitive material, and mechanically tunable surfaces. A different approach is to compensate the degraded antenna performance due to surface distortion by the placement, design, and excitation of the feed. The latter approach is becoming increasingly attractive due to recent advances in monolithic microwave integrated circuits. Feed arrays with many elements can be or will be built compactly and at a reasonable cost.

At any rate, surface error reduction methods and surface error compensation techniques are complementary; each approach can further improve antenna performance independently of the benefits of the other. In this paper, surface error compensation techniques will be examined. Analysis will begin with the assumption that the surface distortion is given; then, methods will be investigated to determine the compensating feed array geometry and element excitations. The sensitivity of the antenna performance to changing surface distortion parameters, for fixed feed array geometries, will then be examined.

For a better understanding of reflector surface error compensation, it is convenient to think of a reflector antenna in the receive mode. Figure 1a depicts a plane wave incident on a perfect parabolic reflector. In the geometric optics limit, all rays will converge to a single point at the focus of the parabola, where they are collected by a single feed element. Figure 1b shows a plane wave incident on a distorted parabolic reflector. In this case, the rays will not converge to a single point, but will be spread over the focal plane. To provide reflector distortion compensation, a feed array must be designed that will capture the energy spread over the focal plane and add it constructively in the feed network. Improvements in antenna performance due to compensation in the receive mode will produce improvements in antenna performance in the transmit mode by reciprocity.

Before designing a feed array to compensate for surface distortion, we must first determine what the important properties of the surface distortion are and how they affect the geometry of the feed array. This will determine the limits of usefulness for feed array compensation. In this section, we will give a simple approximate formula, showing that the amplitude and spacial frequency of the distortion determines the size of the feed array necessary for compensation. If the spacial frequency and amplitude of the surface distortion can be predicted through structural analysis or measurement, an estimate of the feed array area can then be obtained.

Referring to Figure 1c, let us consider an off-set parabolic reflector with focal point at F. The geometry of the undisturbed reflector is completely specified by angles:

θ_{off} = off-set angle of the reflector

θ_{max} = half-angular extent of the reflector surface

Along the y-direction, the surface distortion is described by two parameters:

β = the amplitude of distortion measured radially from the feed, or parallel to the line connecting the vertex V to the focal point F.

N = # of periods in the distortion over the extent of the reflector surface

Then the minimum array size d in the y-direction needed for compensating the surface error is approximately given by

$$d \sim \frac{e\pi N\beta}{\sin \theta_{max}} (1 + \cos \theta_{off}) \qquad (1)$$

where e = 2.718 ..., π = 3.141 ..., d and β have the same length unit, e.g. wavelength. Derivation and more detailed explanation of (1) is given in Section 2.

As an example, assume that $\theta_{max} = 20°$ and $\theta_0 = 45°$. Also assume that the distortion on the reflector can be approximated by sinusoidal shape along y-direction with a period of 1.0 and an amplitude of 0.30 λ. Then the y-direction of the feed array will need to be at least

$$d = \frac{e\pi(0.30)(1.0)}{\sin (20°)} [1 + \cos (45°)] = 12.8 \lambda$$

to fully compensate for the surface distortion. If the distortion is not well approximated by a single sinusoid, it can always decompose into a sum of sinusoids. The component in the summation with the largest βN product could then be used to get an estimate of necessary feed array size. Note

that if the distortion amplitude, or the number of periods over the extent of the reflector surface were doubled, the feed array size in that direction would have to be doubled for complete compensation.

For a complete determination of the feed geometry, the feed element spacing must also be determined. It will be shown that element spacing is related to the focal length and diameter of the reflector.

Once the feed array geometry is known, the amplitude and phase excitations of each array element must be determined. Section 3 will describe two methods for the determination of element excitations: the conjugate field matching technique and the optimum directivity method. The estimated feed geometry and the given reflector distortion profile are combined with the physical optics approximation to calculate field quantities in both methods. Thus, a fairly accurate estimate of antenna performance can be obtained, allowing a fine tuning of the feed array geometry for a given distortion profile.

In practice, the reflector distortion profile is usually not known exactly, and may even be a function of time or orientation of the antenna. It would therefore be necessary to examine how performance, for a given antenna design, is affected by changes in surface distortion. Section 4 utilizes the results of Section 3 to determine how boresight gain is degraded as a function of reflector surface distortion amplitude and spacial frequency for fixed feed array geometries. The results show how sensitive antenna directivity is to changes in the distortion profile.

2. Determination of Feed Geometry

We shall now derive formula (1), which estimates the minimum array dimension needed for compensating the effect of surface distortion. Consider the PEC (perfect electric conductor) reflector shown in Figure 2. An incident plane wave traveling in the $+\hat{z}_R$ direction induces electric currents $\vec{J}_i$ on the reflector surface, which in turn produce the scattered fields $(\vec{E}_s, \vec{H}_s)$ that we wish to determine. This problem can be separated into two parts. The first part concerns the calculation of $(\vec{E}_s, \vec{H}_s)$ on the $z = z_o$ plane. Here we will assume the reflector is large and smooth enough so that geometric optics can be used to determine the scattered fields. In the geometric optics limit, a section of a perfect paraboloid will produce a truncated incoming spherical wave that will converge at the focal point of the paraboloid. If the reflector is distorted, we seek to relate the distortion to effective amplitude and phase errors across the $z = z_o$ plane. The second part of the problem is to determine $(\vec{E}_s, \vec{H}_s)$ for $z < z_o$ once the scattered fields are known over the $z = z_o$ plane. $(\vec{E}_s, \vec{H}_s)$ can be calculated for $z < z_o$ by employing the principles of equivalent sources and images. It should be observed that in order to apply geometric optics, it is assumed that the distortion is smooth enough so that geometric optics can be applied. For distortions that have many local maxima and minima that are not separated by a large number of wavelengths, this assumption breaks down.

In order to gain an intuitive understanding of how surface distortions affect the fields on the $z = z_o$ plane, consider the reflector surface distortion, $\Delta R(\theta,\phi)$, that is superimposed on a perfect paraboloid. The

distorted reflector surface is then given by

$$R'(\theta,\phi) = R(\theta) + \Delta R(\theta,\phi) = 2f\frac{(1-\cos\theta)}{\sin^2\theta} + \Delta R(\theta,\phi) \qquad (2)$$

where $R'(\theta,\phi)$ = distance from the focal point F to a point on the distorted reflector

$R(\theta)$ = distance from F to a point on the perfect paraboloid

f = focal length of the paraboloid.

It is shown in Appendix A that the phase error, $\Delta\gamma(c,\theta,\phi)$, resulting from the distortion $\Delta R(\theta,\phi)$ has maxima, minima, and saddle points occurring at approximately the same values of θ,ϕ as the maxima, minima and saddle points of $\Delta R(\theta,\phi)$. Furthermore, these extreme values are related by

$$\Delta\gamma(c,\theta_i,\phi_i) \cong \frac{2\pi}{\lambda}\Delta R(\theta_i,\phi_i)\,[1+\cos\theta_i] \qquad (3)$$

where (θ_i,ϕ_i) = value of θ and ϕ where extreme values of $\Delta R(\theta,\phi)$ occur

c = constant.

Although $\Delta\gamma(c,\theta,\phi)$ and $\Delta R(\theta,\phi)$ do not have the same shape, they do have approximately the same frequency content, and amplification of their extreme values is related by $[1+\cos\theta_i]$. Note that the variation of ΔR with θ is assumed large compared with the variation of $\cos\theta$ with θ. These properties will prove useful in relating the surface distortion with its resultant phase distortion.

The fields across the $z = z_o$ plane (see Figure 3) can be expressed as the geometric optics (GO) field multiplied by an amplitude distortion weighting function, where the effective phase distortion is added to the phase of the GO field. The amplitude distortion function arises from a change in the undistorted amplitude distribution caused by the curvature of the surface distortion. The scattered electric field can be written for

the x component as

$$E'_{sx}(r_o,\theta_o,\phi_o)\frac{e^{jkr_o}}{r_o}\Bigg|_{z=z_o} = A_{Dx}(r_o,\theta_o,\phi_o)\,A_{GOx}(r_o,\theta_o,\phi_o)\,\frac{e^{jkr_o+j\Delta\gamma(r_o,\theta_o,\phi_o)}}{r_o}\Bigg|_{z=z_o} \tag{4}$$

where $A_{GOx}(\theta_o,\phi_o)\,\frac{e^{jkr_o}}{r_o}\Big|_{z=z_o}$ = GO scattered field for perfect paraboloid

$A_{Dx}(r_o,\theta_o,\phi_o)\Big|_{z=z_o}$ = amplitude distortion weighting function

$e^{j\Delta\gamma(\theta_o,\phi_o,r_o)}\Big|_{z=z_o}$ = phase distortion

A similar expression exists for the y-component. $\Delta\gamma(\theta_o,\phi_o,r_o)$ will be approximated using the properties of its relation with $\Delta R(\theta_o,\phi_o)$.

The fields for $z < z_o$ (Figure 3) can be calculated from the tangential component of the electric field on the aperture plane $z = z_o$. In Appendix B, it is shown that

$$E_{xs}(x_1,y_1) \cong \frac{-jk}{2\pi}\iint_{\sum}\frac{A_{Dx}(r_o,\theta_o,\phi_o)\,A_{GOx}(r_o,\theta_o,\phi_o)}{\sqrt{1-f_x^2-f_y^2}}\,e^{jk\Delta\gamma(\theta_o,\phi_o,r_o)}\,e^{-jk(f_xx_1+f_yy_1)}\,df_x\,df_y \tag{5a}$$

$$E_{ys}(x_1,y_1) \cong \frac{-jk}{2\pi}\iint_{\sum}\frac{A_{Dy}(r_o,\theta_o,\phi_o)\,A_{GOy}(r_o,\theta_o,\phi_o)}{\sqrt{1-f_x^2-f_y^2}}\,e^{jk\Delta\gamma(\theta_o,\phi_o,r_o)}\,e^{-jk(f_xx_1+f_yy_1)}\,df_x\,df_y \tag{5b}$$

where $f_x = \sin\theta_o \cos\phi_o$

$f_y = \sin\theta_o \sin\phi_o$

$\vec{r}_o = x_o\,\hat{x} + y_o\,\hat{y} + z_o\,\hat{z}$

$\vec{r}_1 = x_1\,\hat{x} + y_1\,\hat{y}$

This result was obtained by Rudge et al. [1] using scalar diffraction theory. The derivation in Appendix B is a vector formulation using the same assumptions as in [1].

The x-component of the electric field in the focal plane is the Fourier transform of $A_{Dx}\,A_{GOx}\,e^{-jk\Delta\gamma}$ divided by the amplitude weighting function $\sqrt{1-f_x^2-f_y^2}$. A similar result holds for the y-component. For a perfect parabolic reflector with a large focal length to diameter (f/d) ratio, point source feed, and y-component of electric field equal to zero,

$A_{Dx}\,e^{-jk\Delta\gamma} = 1$ (no distortion)

$\sqrt{1-f_x^2-f_y^2} \cong 1$ for the range of f_x and f_y, $\frac{f}{d} > 2$

$|A_{GOx}| \cong$ constant

and the focal plane distribution reduces to the Fourier transform of the aperture function Σ. Note that for this same reflector in the transmit mode, the far-field pattern due to a point source located at the focal point will also be the Fourier transform of the aperture function Σ. This is the well-known similarity between the far-field pattern and focal-plane distribution. It is interesting to note that this similarity still holds for small amounts of surface distortion.

Geometric optics and equations (5) can be used to calculate the spread of power in the focal plane. Once this distribution is known, the

feed array shape can be choosen to capture most of the incident power in the focal plane. It should be noted that the focal plane power distribution can also be calculated by formulating the transmit problem and applying reciprocity.

To assess the effects of surface distortion on the focal plane distribution, it would be useful to have a closed-form expression that gives a reasonably accurate value for the spread of power in the focal plane, given the properties of the surface distortion profile. To this end, we will use the approach developed by Rudge et al. [6], which assumes a separable aperature distribution given by

$$\frac{A_{Dx}(\theta_o,\phi_o)\, A_{GOx}(\theta_o,\phi_o)}{\sqrt{1 - f_x^2 - f_y^2}}\, e^{-jk\Delta\gamma(\theta_o,\phi_o)} \cong \exp\left\{-j\left[\alpha_x \cos\left(\frac{N_x \pi f_x}{h}\right) + \alpha_y \cos\left(\frac{N_y \pi f_y}{h}\right)\right]\right\} \tag{6}$$

where h is the maximum value of f_x and f_y in the aperture Σ ($h = \sin\theta_{max}$), and Σ has a square shape in f_x and f_y. α_x and α_y are the amplitudes of the phase distortion. Although (5) seems to be an over-simplification, we can think of decomposing $\Delta\gamma$ into its frequency components, such that

$$e^{-jk\Delta\gamma} = \prod_{p=1}^{\infty} \prod_{q=1}^{\infty} \exp\left\{-j\left[\alpha_{xp} \cos\frac{N_{xp}\pi f_x}{h} + \alpha_{yq} \cos\left(\frac{N_{yq}\pi f_y}{h}\right)\right]\right\} \tag{7}$$

The Fourier transform of $A_{Dx}\, A_{GOx}\, e^{-jk\Delta\gamma}$ will equal the convolution of all Fourier transforms of $e^{-j\left[\beta_{xn} \cos\frac{N_{xn}\pi f_x}{h} + \beta_{yn} \cos\left(\frac{N_{ym}\pi f_y}{h}\right)\right]}$, the Fourier transform of A_{Dx}, and the Fourier transform of A_{GOx}. Generally, distortions caused by temperature gradients and gravitational effects will be dominated by a small number of spacial frequency components, and the product of (7)

can be truncated after a few terms. Substituting the right-hand side of (6) into (5a) yields

$$E_{sx}(x_1,y_1) = \frac{-jk}{2\pi}\int_{-h}^{h} e^{i\alpha_x\cos(\frac{N_x\pi f_x}{h})}\, e^{-jkf_x x_1}df_x \int_{-h}^{h} e^{i\alpha_y\cos(\frac{N_y\pi f_y}{h})}\, e^{-jkf_y y_1}df_y \tag{8}$$

We need to evaluate the integral $\int_{-h}^{h} e^{i\alpha_x\cos(\frac{N_x\pi f_x}{h})}e^{-jkf_x x_1}df_x$, (the integral over f_y has a similar form). Evaluating yields

$$\int_{-h}^{h} e^{-\alpha_x\cos(\frac{N_x\pi f_x}{h})}e^{-jkf_x x_1}df_x$$

$$= 2h\, J_o(\beta_x)\frac{\sin khx_1}{khx_1} + 2h\sum_{n=0}^{\infty}(i)^n J_n(\alpha_x)\left[\frac{\sin[khx_1-nN_x\pi]}{khx_1-nN_x\pi} + \frac{\sin[khx_1+nN_x\pi]}{khx_1-nN_x\pi}\right] \tag{9}$$

If the magnitude of the phase distortion $\alpha_x = 0$, a sinc function is obtained. As α_x increases, the sinc function amplitude decreases as a function of $J_o(\alpha_x)$, and other sinc functions displaced by $\pm\frac{nN_x\pi}{kh}$ in the x_1 direction emerge with amplitudes governed by $J_n(\alpha_x)$. The emergence of these sinc functions corresponds to the spreading of power in the focal plane as the amplitude of the distortion is increased. Note that the larger N_x is, the larger the distance is between sinc functions for given values of α_x. Hence, if the distortion has a high spacial frequency content (short correlation period), the power will be spread over a larger portion of the focal plane than if it had a lower spacial frequency content for the same value of α_x. We can quantify this observation by determining how large n has to be for a given α_x so that $|J_n(\alpha_x)|$ is negligible. For $n>\beta>2$ we have

$$|J_n(\alpha_x)| < \frac{i}{ni}\left(\frac{\alpha_x}{2}\right)n+\left(\frac{\alpha_x}{2}\right) \cong \frac{(\alpha_x/2)^{\alpha_x/2}}{\sqrt{2\pi n}}\left(\frac{e\alpha_x}{2n}\right)^n \tag{10}$$

Therefore, $|J_n(\alpha_x)|$ goes rapidly to zero for $n > \frac{e\alpha_x}{2}$ and we can write

$$n_{max}N_x\pi = k\, x_{1max}\, h = \frac{e\alpha_x}{2} N_x\pi \tag{11}$$

where we assume

$$J_{nmax}(\alpha_x)\left[\frac{\sin[khx_{1max}-n_{max}N_x\pi]}{kh_{xmax}-n_{max}N_x\pi} + \frac{\sin[khx_{1max}+n_{max}N_x\pi]}{khx_{1max}+n_{max}N_x\pi}\right]$$

is the last contributing pair of sinc functions in the focal plane as n increases. We now rearrange (11) to obtain an expression for the width d_{fx} in the focal plane over which the power will be spread given α_x and N_x.

$$d_x = 2x_{1max} = \frac{e\alpha_x N_x \lambda}{2 \sin \theta_{max}} \tag{12}$$

Since the spacial frequency of the surface distortion profile is close to the spacial frequency of its resultant phase distortion, and phase distortion amplitude can be approximately related to surface distortion amplitude by equation (3), we can write

$$d_x \cong \frac{e\pi N\beta_x}{\sin \theta_{max}} \quad (1 + \cos \theta_i) \tag{13}$$

Here β_x is the peak amplitude of the given frequency component of surface distortion (in λ), and θ_i can be approximated as the angle, θ_{off} in Figure 1, between the z-axis and the line connecting the center of the reflector to the focal point. ($\theta_i \cong 0$ for prime focus reflectors; $\theta_i \neq 0$ for offset

reflectors.) Equation (13) gives a simple relation between the surface distortion properties and how large the feed array needs to be to capture the incident power in the focal plane. As we shall see, this formula gives a fairly good estimate of array size when we compare the results with a more exact numerical analysis using a separable surface distortion. Note that if the estimate of d from Equation (13) is too large, the use of compensating feed array is not feasible.

With the feed array shape determined, we must now determine the element spacing for the complete characterization of the feed geometry. The feed element spacing should be as large as possible provided that no grating lobes fall inside the angular extent of the reflector as measured from the focus. This choice will minimize the number of feed elements without significantly affecting antenna performance, as will be shown in the calculated results.

3. Determination of Feed Element Excitations

With an understanding of how the geometry of the feed array is estimated from the surface distortion, it is now possible to determine the amplitude and phase excitations of the feed elements for compensating degraded antenna patterns. In this analysis, it will be convenient to think of the reflector antenna in the transmit mode. Let us consider a distorted parabolic reflector antenna with a feed array of N elements. The complex excitation coefficients, represented by a column vector $\bar{I}$,

$$\bar{I} = [I_1, I_2, \ldots I_N]^T \tag{14}$$

are to be determined. To this end, let us first calculate the far field (secondary pattern) of the distorted reflector due to the n^{th} element, namely due to the following array excitation

$$I_m = 1, \text{ and all other } I_n = 0 \tag{15}$$

That far field is denoted by

$$\vec{E}(\vec{r}) \sim \frac{e^{-jkr}}{r} [\vec{R}\, E_m(\theta,\phi) + \vec{C}\, F_m(\theta,\phi)] \tag{16}$$

Here (r,θ,ϕ) is the spherical coordinate of the observation point. $(\vec{R},\vec{C})$ are unitary complex vectors describing the (reference, cross) polarizations of the antenna. An example of E_m with $m = 2$ is sketched in Figure 4. The column vector

$$\vec{E}(\theta,\phi) = [E_1, E_2, \ldots E_N]^T \tag{17}$$

represents the reference-polarization radiation in direction (θ,ϕ) of the distorted reflector due to each individual element in the feed array. In

the present paper, we calculate $\vec{E}(\theta,\phi)$ by the standard physical optics integration method.

There are two ways for determining excitation $\bar{I}$ to improve a degraded pattern. The first one is the conjugate field matching method (CFM), in which we set*

$$\bar{I} = \bar{E}^* \ (\theta = \theta_{beam}, \ \phi = \phi_{beam}) \tag{18}$$

Here $(\theta_{beam}, \phi_{beam})$ is the desired main beam direction of the antenna. This method has been known for more than ten years, and is widely used in practice [5], [10] - [18]. It has been pointed out [15] that, while CFM gives good results, it is not an optimum solution in any sense. A truly optimum solution which maximizes the antenna directivity in direction $(\theta_{beam}, \phi_{beam})$ is given by [8]

$$\bar{I} = (\bar{\bar{A}}^*)^{-1} \ \bar{E}^*(\theta = \theta_{beam}, \ \phi = \phi_{beam}) \tag{19}$$

Here $\bar{\bar{A}}$ is a N × N square matrix describing the coupling between primary patterns of the feed elements. The presence of $\bar{\bar{A}}$ is due to the fact that the total power radiated by the feed array is <u>not</u> equal to the sum of the powers radiated by the individual feed elements [19], a statement that superposition of power does not hold in general. Now, for the special case that spacing between feed elements is large in wavelength, couplings between element patterns are small. Then $\bar{\bar{A}}$ is nearly diagonal and the optimum solution in (19) reduces to CFM in (18).

---

* Within a proportional constant.

The above two methods for determining feed array excitations are originally used for compensating degraded secondary patterns arising from off-focus feeds. In the next section, we will show that they work just as well for compensating the other cause of degraded pattern: reflection surface distortion.

4. Calculated Results

To outline a method for designing a distortion compensating feed array, we will take a specific example of the reflector shown in Figure 5 with the distortion shown in Figure 6a and Table 1. Note that parameters (N_x, N_y) describe ripple numbers along (x,y) directions, respectively. Parameters (β_x, β_y) describe the corresponding ripple amplitude. First, the focal plane distribution due to a plane wave incident from the boresight direction is calculated. This can be done using the method of Section 2, or applying reciprocity to the solution of the transmitting problem. From this analysis, the array of Figure 7a was found to capture most of the energy spread over the focal plane. The element spacing was choosen such that no grating lobes of the feed array fell on the reflector. The optimum directivity method was then applied to determine the element weights, and the compensated far-field patterns shown in Figure 8 were obtained. These compensated patterns can be compared with the patterns for the undistorted reflector using a single feed (Figure 9) and the distorted reflector using a single feed (Figure 10). All but 1.7 dB of the undistorted reflector gain were recovered with the array feed.

As noted before, the actual distortion profile is usually not known exactly. It would therefore be interesting to see how the antenna gain degrades for a fixed feed array geometry when properties of the surface distortion are varied. Using the feed geometry in Figure 7 and surface distortion of Figure 6a, the degradation of boresight optimum directivity with increasing distortion amplitude is shown for three different feed array areas in Figure 11a. From these results, it is evident that the feed array area increases approximately as the square of distortion

amplitude to maintain a given value of gain (i.e., 55 dB). This is in agreement with the analysis of Section 2. Figure 11b shows similar results for the case when conjugate field matching is used instead of the optimum directivity method. Note that the values of directivity are slightly lower (the single element case is the same for both the CFM and the optimum methods). Figure 12 depicts peak directivity degradation as distortion amplitude increases for two arrays of the same area but with a different number of elements (i.e., different spacings). Not much improvement is gained by using smaller and more closely spaced elements in a given feed array area. The three-element array corresponds to the largest element spacing allowed without having grating lobes fall on the reflector. Figure 13 shows the decrease in peak gain as a function of distortion amplitude for two different distortion profiles (Figures 6a and 6b). The feed array is the same (Figure 7b) in each case. The distortion with higher spacial frequency cannot be compensated for as well as the distortion of lower spacial frequency. Since the distortions are separable, Equation (1) can be used to estimate the maximum value of distortion amplitude at which full compensation can be realized. Rearranging Equation (1), we find that this maximum distortion amplitude is given by

$$\beta = \frac{d \sin (\theta_{max})}{e\pi N[1 + \cos (\theta_{off})]}$$

For the reflector geometry used in the numerical results

$$\theta_{max} = 20°$$

$$\theta_o = 43°$$

$$d = 8 \lambda$$

therefore

$$\beta = \frac{0.185\ \lambda}{N}$$

$$= \begin{cases} 0.16\ \lambda, & \text{for } N = 1.167 \quad \text{(Distortion 2)} \\ 0.24\ \lambda, & \text{for } N = 0.770 \quad \text{(Distortion 1)} \end{cases}$$

These values are marked by points A and B in Figure 13. Numerically calculated gains begin to fall off shortly after these values. This verifies the validity of Equation (1).

In all the cases presented thus far, the feed array amplitude and phase weighting are continuous. As a matter of practical importance, it would be interesting to know how phase and amplitude quantization affects the performance of the antenna. To determine this effect, a plot was made (Figure 14) of the degradation in peak boresight directivity as a function of quantization. The horizontal axis shows the number of bits of linear quantized phase and amplitude. (A 3-bit quantization means 2^3 steps in phase, and 2^3 steps in amplitude.) This case is for the 25-element feed array of Figure 7b and distortion function #2 with $\beta_x = \beta_y = 0.175\ \lambda$. Note that a quantization of as few as 3 bits produces a loss of only 0.60 dB from the continuous amplitude and phase optimum peak boresight directivity. A 5-bit quantization is sufficient for practical purposes.

From these results, it is apparent that for a given array, the loss of gain can be compensated for provided the distortion amplitude and spacial frequency remain within certain limits. Therefore, by designing for the maximum distortion amplitude and maximum distortion spacial frequency, the compensating feed array should work well for the continuum of surface distortion profiles up to and including those extremes.

5. Conclusion

The facets of reflector surface distortion compensation were explored by first assuming the reflector distortion was given and then designing the compensating feed array. We also examined the sensitivity of boresight directivity to changing surface distortion parameters for fixed feed-array geometries. It was found that feed array compensation is feasible only for distortions with low spacial frequency content, such as those induced by thermal and gravitational effects. The optimum directivity method for determining element excitations was found to yield slightly better values of directivity than those for the conjugate field matching technique. However, the CFM technique lends itself to simple realization in hardware, and may be very useful in an adaptive implementation. In view of these results, distortion compensation using an array feed is indeed a reasonable approach to improving antenna performance for large, space-based reflector antennas that are not easily accessible for tuning and have time-dependent surface distortions. This is particularly true when considering the recent advances in MMIC feed array technology.

REFERENCES

1. Ruze, J.: Antenna Tolerance Theory - A Review. Proc. IEEE, vol. 54, no. 4, Apr. 1966, pp. 633-640.

2. Rusch, W.V.T.: The Current State of the Reflector Antenna Art. IEEE Trans. Antennas Propag., vol. AP-32, no. 4, Apr. 1984, pp. 313-329.

3. Ling, H.; Lo, Y.T.; and Rahmat-Samii, Y.: Reflector Sidelobe Degradation Due to Random Surface Errors. IEEE Trans. Antennas Propag., vol. AP-34, no. 2, Feb. 1986, pp. 164-172.

4. Steinbach, R.E.; and S.R. Winegar: Interdisciplinary Design Analysis of a Precision Spacecraft Antenna. 26th Structures, Structural Dynamics and Materials Conference, Part 1, AIAA, 1985, pp. 704-713.

5. Acosta, R.J.: Compensation of Reflector Surface Distortion Using Conjugate Field Matching. IEEE International Symposium Digest on Antennas and Propagation, Vol. 1, IEEE, 1986, pp. 259-262.

6. Rudge, A.W.; and Davies, D.E.N.: Electronically Controllable Primary Feed for Profile-Error Compensation of Large Parabolic Reflectors. Proc. IEE, vol. 117, no. 2, Feb. 1970, pp. 351-358.

7. Ludwig, A.C.: The Definition of Cross Polarization. IEEE Trans. Antennas Propag., vol. AP-21, no. 1, Jan. 1973, pp. 116-119.

8. Lam, P.T., et al.: Directivity Optimization of a Reflector Antenna with Cluster Feeds: A Closed Form Solution. IEEE Trans. Antennas Propag., vol. AP-33, no. 11, Nov. 1985, pp. 1163-1174.

9. Harrington, R.F.: Time Harmonic Electromagnetic Fields. McGraw-Hill, 1961, pp. 110-113.

10. Midgley, D.: A Theory of Receiving Aerials Applied to the Reradiation of an Electromagnetic Horn. Proc. IEE, vol. 108B, 1961, pp. 645-650.

11. Visocekas, R.: Non-Cassegrainian Indirect System for Aerial Illumination. Proc. IEE, vol. 111, 1964, pp. 1969-1975.

12. Minnett, H.C.; and Thomas, B.: Fields in the Image Space of Symmetrical Focusing Reflectors. Proc. IEE, vol. 115, no. 10, Oct. 1968, pp. 1419-1430.

13. Rudge, A.W.; and Withers, M.J.: Design of Flared-Horn Primary Feeds for Parabolic Reflector Antennas. Proc. IEE, vol. 117, no. 9, Sept. 1970, pp. 1741-1749.

14. Luh, H.H.S.: On the Radiation Pattern of a Multibeam Antenna. IEEE Trans. Antennas Propag., vol. AP-24, no. 1, Jan. 1976, pp. 101-102.

15. Rahmat-Samii, Y.; and Lee, S.W.: Application of the Conjugate Field Matching Technique to Reflector Antennas - A Critical Review. URSI Digest, 1981, p. 85.

16. Mrstik, A.V.; and Smith, P.G.: Scanning Capabilities of Large Parabolic Cylinder Reflector Antennas with Phased-Array Feeds. IEEE Trans. Antennas Propag., vol. AP-29, no. 3, May 1981, pp. 455-462.

17. Hung, C.C.; and Mittra, R.: Secondary Pattern and Focal Region Distribution of Reflector Antennas Under Wide-Angle Scanning. IEEE Trans. Antennas Propag., vol. AP-31, no. 5, Sept. 1983, pp. 756-763.

18. Jong, H.Y., et al.: Analysis of Paraboloidal Reflector Fields Under Oblique Incidence. AP Digest, vol. 1, 1984, pp. 305-308.

19. Rahmat-Samii, Y.; and Lee, S.W.: Directivity of Planar Array Feeds for Satellite Reflector Applications. IEEE Trans. Antennas Propag., vol. AP-31, no. 3, May 1983, pp. 463-470.

Appendix A: Relation Between Surface Distortion and Resultant Phase Distortion

Let $R = 2f \frac{(1 - \cos\theta)}{\sin^2\theta}$ = distance from F to a point (R,θ,ϕ) on the perfect parabolic reflector

$R' = 2f \frac{(1 - \cos\theta)}{\sin^2\theta} + \Delta R(\theta,\phi)$ = distance from F to a point (R',θ,ϕ) on the distorted reflector

The normal to the perfect reflector at the point (R,θ,ϕ) has direction given by

$$\vec{V} = -\hat{r} + \hat{\theta}\,\frac{2f}{R}\,\frac{(1 - \cos\theta)^2}{\sin^3\theta} \qquad (A.1)$$

The normal to the distorted reflector at the point (R',θ,ϕ) has direction given by

$$\vec{V}' = -\hat{r} + \hat{\theta}\left[\frac{2f}{R'}\,\frac{(1 - \cos\theta)^2}{\sin^3\theta} + \frac{1}{R'}\,\frac{\partial\Delta R(\theta,\phi)}{\partial\theta}\right] + \hat{\phi}\,\frac{1}{R'\sin\theta}\left[\frac{\partial\Delta R(\theta,\phi)}{\partial\phi}\right] \qquad (A.2)$$

For values of (θ,ϕ) where $\Delta R(\theta,\phi)$ is a local maximum, minimum or saddle point, we have

$$\frac{\partial\Delta R(\theta,\phi)}{\partial\theta} = \frac{\partial\Delta R(\theta,\phi)}{\partial\phi} = 0 \qquad (A.3)$$

Therefore,

$$\vec{V}' = -\hat{r} + \hat{\theta}\,\frac{2f}{R'}\,\frac{(1 - \cos\theta)^2}{\sin^3\theta} \qquad (A.4)$$

$$= -\hat{r} + \hat{\theta}\,\frac{2f}{R}\left[1 - \frac{\Delta R}{R} + \left(\frac{\Delta R}{R}\right)^2 - \left(\frac{\Delta R}{R}\right)^3 + \ldots\right]\frac{(1 - \cos\theta)^2}{\sin^3\theta}$$

If $\frac{\Delta R}{R} \ll 1$ [+*], then $\vec{V}' \cong \vec{V}$, and the normals for the perfect and distorted reflectors are approximately equal for values of (θ,ϕ) where $\Delta R(\theta,\phi)$ has extreme values. The approximation becomes an exact equality as $\theta \to 0$.

Referring to Figure 15, the difference in path lengths between $|\vec{PQ}| + |\vec{QU}|$ and $|\vec{P'Q'}| + |\vec{Q'U}|$ is given by

$$|\vec{PQ}| + |\vec{QU}| - |\vec{P'Q'}| - |\vec{Q'U}| \cong \Delta R(\theta,\phi)\ [1 + \cos\theta] \tag{A.5}$$

for the values (θ,ϕ) corresponding to the extremes of $\Delta R(\theta,\phi)$. Since the phases at P and P' are equal, then the difference between the phase at u for the perfect reflector and the phase at u for the distorted reflector is given by

$$\Delta\gamma(c,\theta,\phi) \cong \frac{2\pi}{\lambda}\ \Delta R(\theta,\phi)\ [1 + \cos\theta] \tag{A.6}$$

Now if the sphere r = c is chosen large enough so that none of the reflected rays cross before intersecting the sphere, then in the geometric optics limit $\Delta\gamma(c,\theta,\phi)$ is at an extreme value on the sphere r = c. This is in fact true because a ray is normal to its equiphase surface, and $\nabla\ \Delta\gamma(r,\theta,\phi) \propto \hat{r}$ at r = c. Therefore,

$$\frac{1}{c}\ \frac{\partial\Delta\gamma(c,\theta,\phi)}{\partial\theta} = 0 \tag{A.7}$$

$$\frac{1}{c\ \sin\theta}\ \frac{\partial\Delta\gamma(c,\theta,\phi)}{\partial\phi} = 0 \tag{A.8}$$

Since the phase distribution on r = c due to reflected rays from the perfect parabola is constant, and we are interested only in relative phase on the sphere r = c, $\Delta\gamma(c,\theta,\phi)$ is the phase distortion due to the surface distortion $\Delta R(\theta,\phi)$.

+ A typical value for $\frac{\Delta R}{R}$ for a sloppy reflector surface is around 0.001 (assuming $\Delta R \cong 60$ mills and R = 60 inches). For these values, the change in $\hat{\theta}$ component will be less than 0.0006 if the reflector surface does not extend past $\theta = 60°$.

* If ΔR changes 60 mills for a change in θ of 25°, the change in $\hat{\theta}$ due to the slope of the distortion is around 0.002.

$\Delta\gamma(c,\theta,\phi)$ and $\Delta R(\theta,\phi)$ have maxima, minima and saddle points occurring at approximately the same values of (θ,ϕ). It is therefore reasonable to assume that $\Delta\gamma(c,\theta,\phi)$ and $\Delta R(\theta,\phi)$ have approximately the same frequency content in θ and ϕ. Notice also that the maxima, minima and saddle points of $\Delta\gamma$ occur at values independent of r, for $r > c$.

Appendix B: Calculation of Focal Plane Fields

Consider Figure 2; the induced current $\vec{J}_i$ on the reflector surface produces scattered fields $(\vec{E}_s, \vec{H}_s)$. $\vec{J}_i$ can be replaced by the equivalent sources $\vec{J}_s = \hat{n} \times \vec{H}_s$ and $\vec{M}_s = \vec{E}_s \times \hat{n}$ on $z = z_o$ plane to obtain the same scattered fields $\vec{E}_s$, $\vec{H}_s$ for $z < z_o$ as produced by the induced current $\vec{J}_i$. By applying the image theory, the fields $(\vec{E}_s, \vec{H}_s)$ for $z < z_o$ can be calculated from the magnetic source $\vec{M}_s = 2\vec{E}_s \times \hat{n}$ alone. It can be shown [4] (see Figure 3) that

$$\vec{E}(\vec{r}_1) = - \nabla \times \int\int_{\Sigma} \frac{e^{-jkr_{10}}}{2\pi r_{10}} \vec{E}(\vec{r}_o) \times \hat{z} \, ds_o \qquad (B.1)$$

where $\vec{E}(\vec{r}_o)$ = electric field on the aperture Σ

$\vec{E}(\vec{r}_1)$ = electric field for $z < z_o$

ds_o = element of surface area on the $z = z_o$ plane.

If we approximate $\vec{E}(\vec{r}_o)$ by a vector weighting function times an incoming spherical wave, we have

$$\vec{E}(r_1) = - \nabla \times \int\int_{\Sigma} \frac{e^{-jkr_{10}}}{2\pi r_{10}} \vec{E}_s'(r_o,\theta_o,\phi_o) \frac{e^{jkr_o}}{r_o} \times \hat{z} \, ds_o \qquad (B.2)$$

$$= - \frac{1}{2\pi} \nabla \times \int\int_{\Sigma} \frac{e^{-jk(r_{10}-r_o)}}{r_{10} r_o} \vec{E}_s'(\theta_o,\phi_o) \times \hat{z} \, ds_o$$

where $\vec{E}_s'(r_o,\theta_o,\phi_o) = \hat{x} E_{sx}'(r_o,\theta_o,\phi_o) + \hat{y} E_{sy}'(r_o,\theta_o,\phi_o) + \hat{z} E_{sy}'(r_o,\theta_o,\phi_o)$

$r_o = |\vec{r}_o|$

$r_1 = |\vec{r}_1|$

Note from Figure 3 we have, by the law of cosines,

$$r_{10}^2 = r_o^2 + r_1^2 - 2r_1 r_o \sin\theta_1 \sin\theta_o \cos(\phi_o - \phi_1) - 2r_1 r_o \cos\theta_1 \cos\theta_o$$

Therefore,

$$\frac{r_{10}^2}{r_o^2} = 1 + \frac{r_1^2}{r_o^2} - 2\frac{r_1}{r_o}\left[\sin\theta_1 \sin\theta_o \cos(\phi_o-\phi_1) + \cos\theta_1 \cos\theta_o\right]$$

Assuming $\frac{r_1}{r_o} \ll 1$

$$r_{10}^2 - r_o^2 \cong 2r_1 r_o \left[\sin\theta_1 \sin\theta_o \cos(\phi_o-\phi_1) + \cos\theta_1 \cos\theta_o\right]$$

$$r_{10} - r_o \cong r_1 \left[\sin\theta_1 \sin\theta_o \cos(\phi_o-\phi_1) - \cos\theta_1 \cos\theta_o\right] \qquad (B.3)$$

$$\cong x_1 \sin\theta_o \cos\phi_o + y_1 \sin\theta_o \sin\phi_o + z_1 \cos\theta_o$$

$$= x_1 f_x + y_1 f_y + z_1 f_z$$

where $f_x = \sin\theta_o \cos\phi_o$ (B.4)

$f_y = \sin\theta_o \sin\phi_o$ (B.5)

$f_z = \cos\theta_o$. (B.6)

Substituting (B.3) into (B.2) yields

$$\vec{E}(r_1) \cong -\frac{1}{2\pi}\iint_{\sum} \nabla\times\left[\frac{e^{-jk(x_1 f_x + y_1 f_y + z_1 f_z)}}{r_o^2}\ \vec{E}_s'(\theta_o,\phi_o,r_o)\times\hat{z}\right] ds_o \qquad (B.7)$$

Crossing $\vec{E}_s(\theta_o,\phi_o,r_o)$ with $\hat{z}$ and performing the curl operation yield

$$\vec{E}(r_1) = -\frac{1}{2\pi}\iint_{\sum}\Big[-jk(\sin\theta_o\cos\phi_o E_{xs}' + \sin\theta_o \sin\phi_o E_{ys}')\,\hat{z}$$

$$+ jk\cos\theta_o E_{ys}'\,\hat{y} + jk\cos\theta_o E_{xs}'\,\hat{x}\Big]\frac{e^{-jk(x_1 f_x + y_1 f_x + z_1 f_z)}}{r_o^2} ds_o$$

(B.8)

Note that

$ds_o = \rho_o\, d\rho_o\, d\phi_o$ where $\rho_o = r_o \sin\theta_o$

$z_o = r_o \cos\theta_o$

Therefore,

$$ds_o = z_o^2 \frac{\sin\theta_o}{\cos^3\theta_o} d\theta_o d\phi_o = r_o^2 \frac{\sin\theta_o}{\cos\theta_o} d\theta_o d\phi_o \qquad (B.9)$$

Substituting (B.9) into (B.8) and realizing $z_1 = 0$ in the focal plane, we have

$$\vec{E}(r_1) = -\frac{jk}{2\pi}\iint_{\Sigma}[-(\tan\theta_o \cos\phi_o E_{xs} + \tan\theta_o \sin\phi_o E_{ys})\,\hat{z} + E_{ys}\,\hat{y} + E_{xs}\,\hat{x}]\, e^{-jk(x_1 f_x + y_1 f_y)} \sin\theta_o\, d\theta_o\, d\phi_o \qquad (B.10)$$

$$= -\frac{jk}{2\pi}\iint_{\Sigma}[-(\frac{f_x}{\sqrt{1 - f_x^2 - f_y^2}} E_{xs} + \frac{f_y}{\sqrt{1 - f_x^2 - f_y^2}} E_{ys})\,\hat{z} + E_{ys}\,\hat{y} + E_{xs}\,\hat{x}\,] \frac{1}{\sqrt{1 - f_x^2 - f_y^2}} e^{-jk(x_1 f_x + y_1 f_y)}\, df_x df_y \qquad (B.11)$$

TABLE 1. Distortion Function Data

(x in inches, y in inches, and Δ z in wavelengths @ 30 GHz)

Distortion Function	Equation	Sinusoidal Approximation
#1	$\Delta z = \beta_x(-0.0000001574x^4) + \beta_y(12.38 - 0.4138y + 0.004100y^2 - 0.00001226y^3)$ $0 < \beta_x, \beta_y < 1.0\ \lambda$	$\Delta z = \beta_y \cos[\frac{N_y\pi}{y_{max}}(y-145.8)]$ (x variation neglected) $N_y = 0.7697$ $y_{max} = 52.8$ in.
#2	$\Delta z = \beta_x(1.0 - 0.001953x^2 + 0.000000474x^4) + \beta_y(12.38 - 0.4138y + 0.004100y^2 - 0.00001226y^3)$ $0 < \beta_x, \beta_y < 1.0\ \lambda$	$\Delta z = \beta_x \cos(\frac{N_x\pi}{x_{max}}x) + \beta_y \cos[\frac{N_y\pi}{y_{max}}(y-145.8)]$ $N_x = 1.167$ $N_y = 0.7697$ $x_{max} = y_{max} = 52.8$ in.

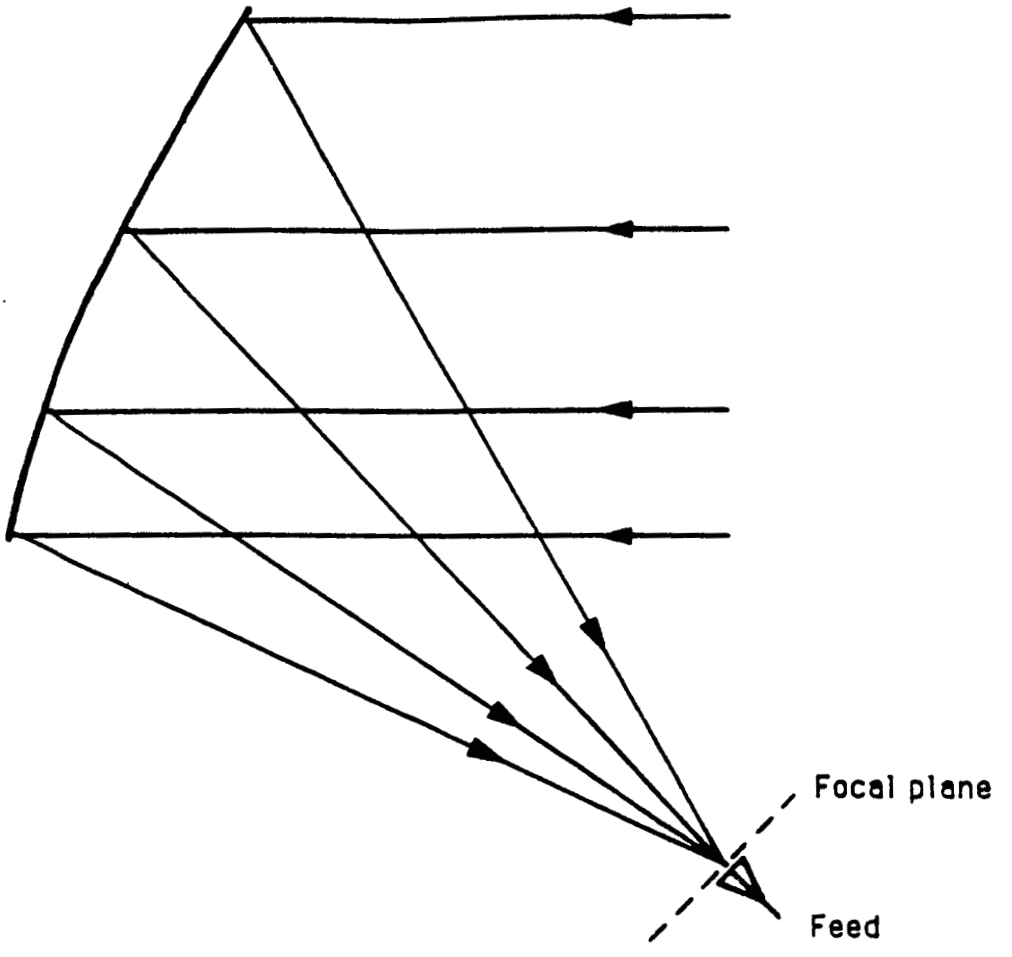

FIGURE 1a. Rays Converging at the Focus of a Perfect Parabolic Reflector

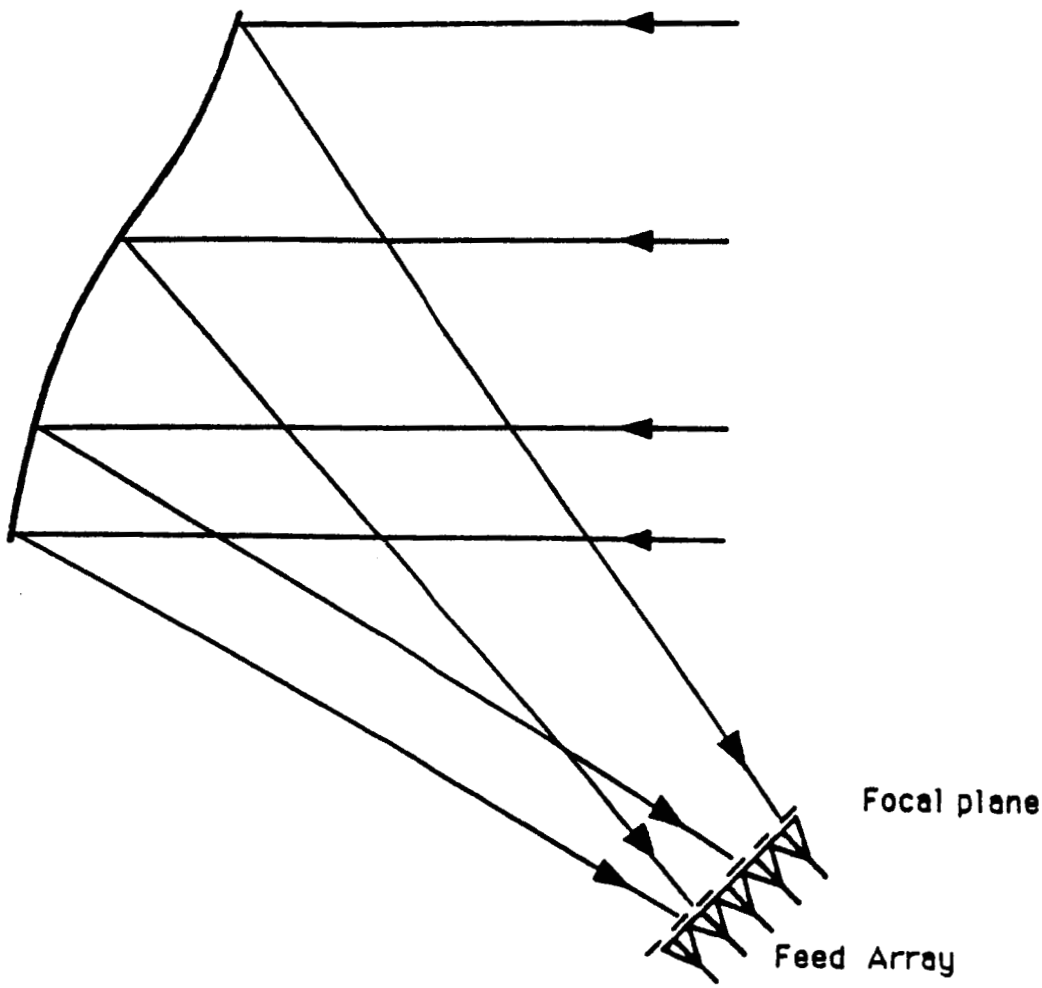

FIGURE 1b. Rays Spread Over the Focal Plane of a Distorted Reflector

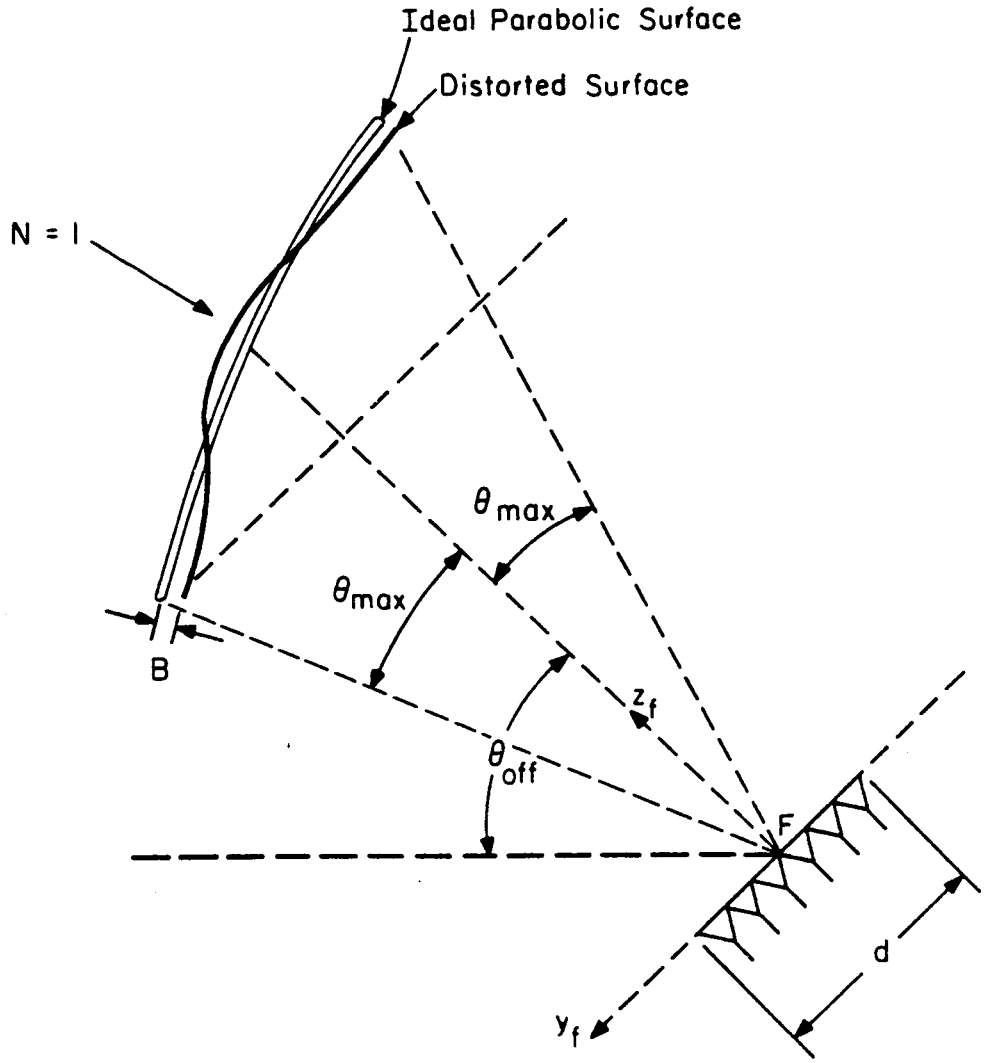

FIGURE 1c. Reflector - Feed Geometry for Equation (1)

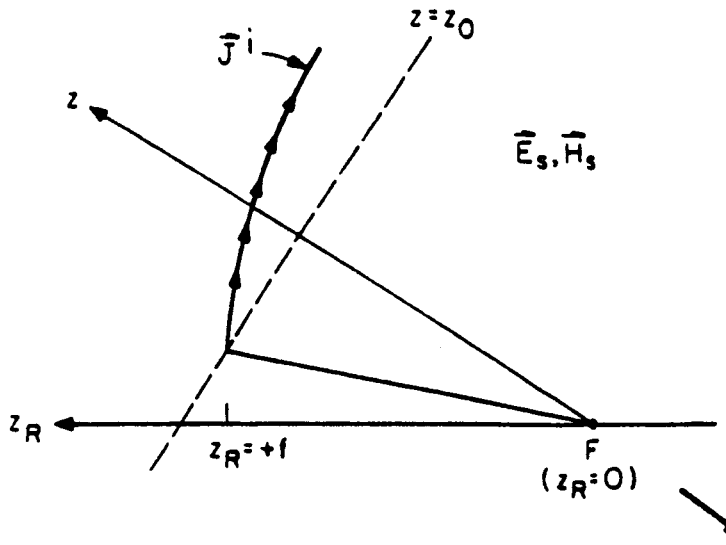

(a) Induced current J^i on the reflector surface produces scattered fields E_s, H_s.

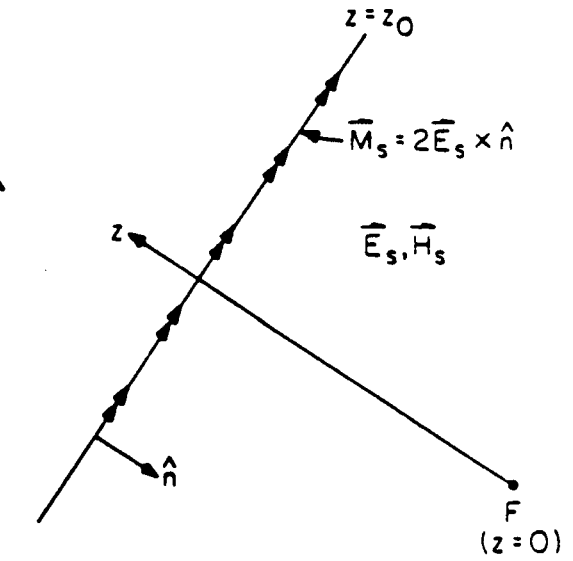

(b) Equivalent magnetic current M_s produces scattered fields E_s, H_s for z less than z_0.

FIGURE 2. Geometry for the Problem of Scattering from a Reflecting Surface.

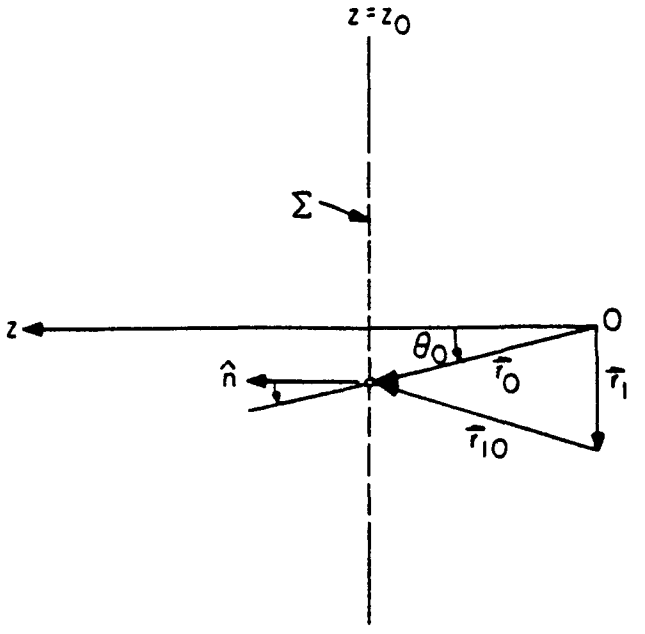

FIGURE 3. Geometry for the Focal Plane Electric Field Calculation.

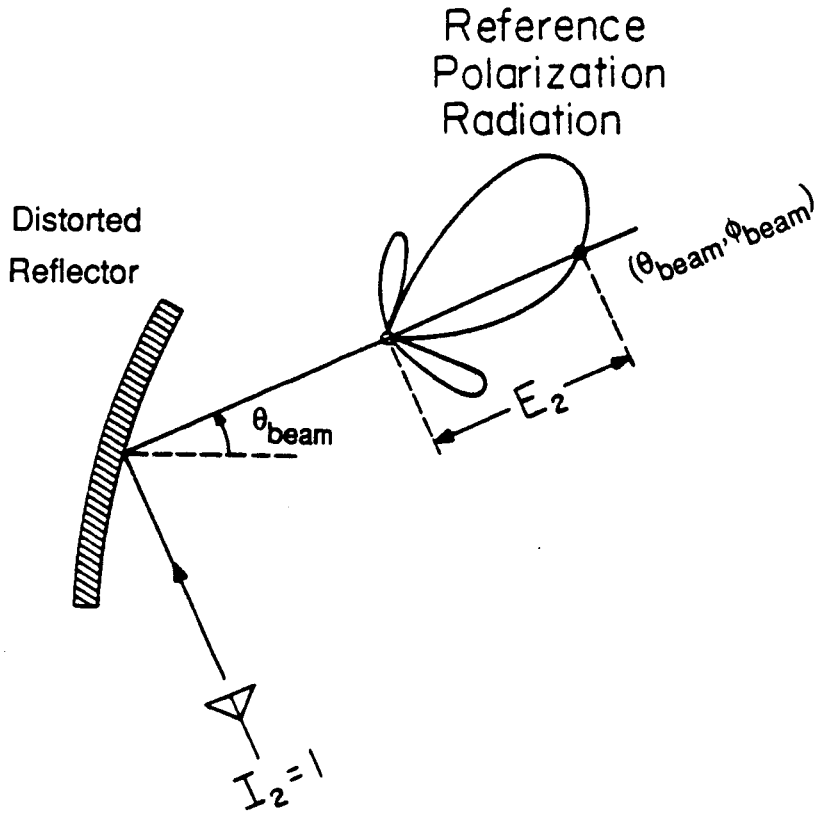

FIGURE 4. The Reference-Polarization Secondary Pattern in direction $(\theta_{beam},\phi_{beam})$ is E_2 when only Feed Element 2 is Excited with $I_2 = 1.0$.

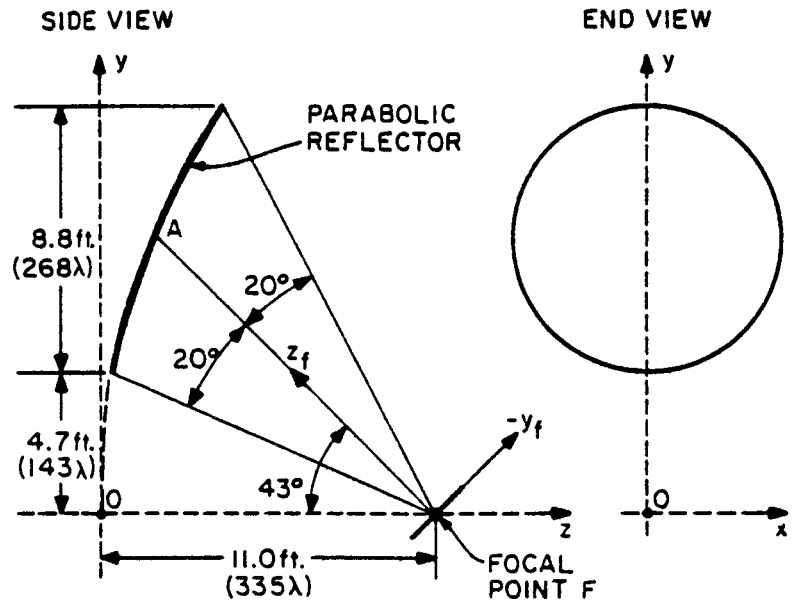

FIGURE 5. Reflector Geometry Used to Obtain the Numerical Results. The feed array is located at the $z_f = 0$ plane. The frequency is 30 Ghz ($\lambda = 0.3937$").

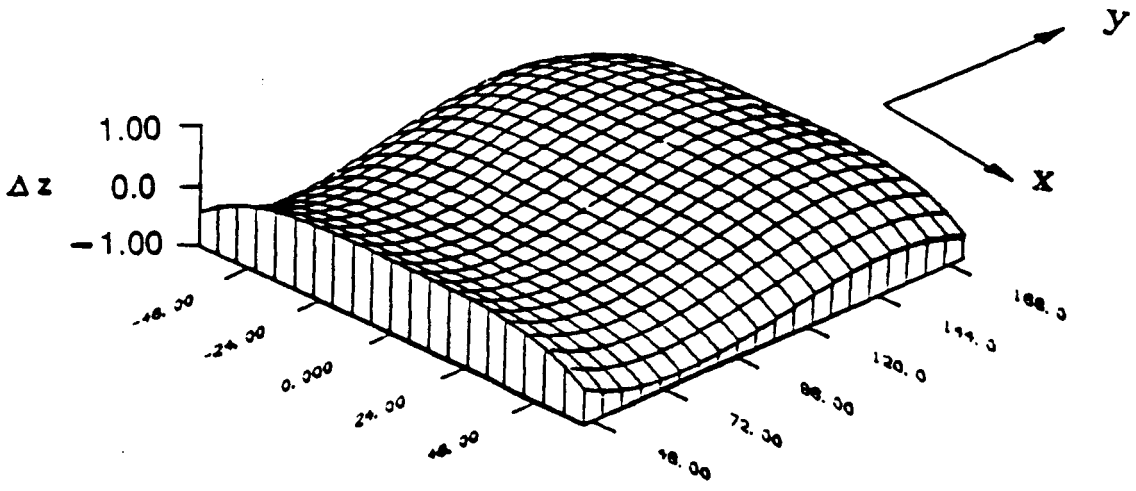

(a) distortion function #1 plotted for $\beta_x = \beta_y = 1\lambda$

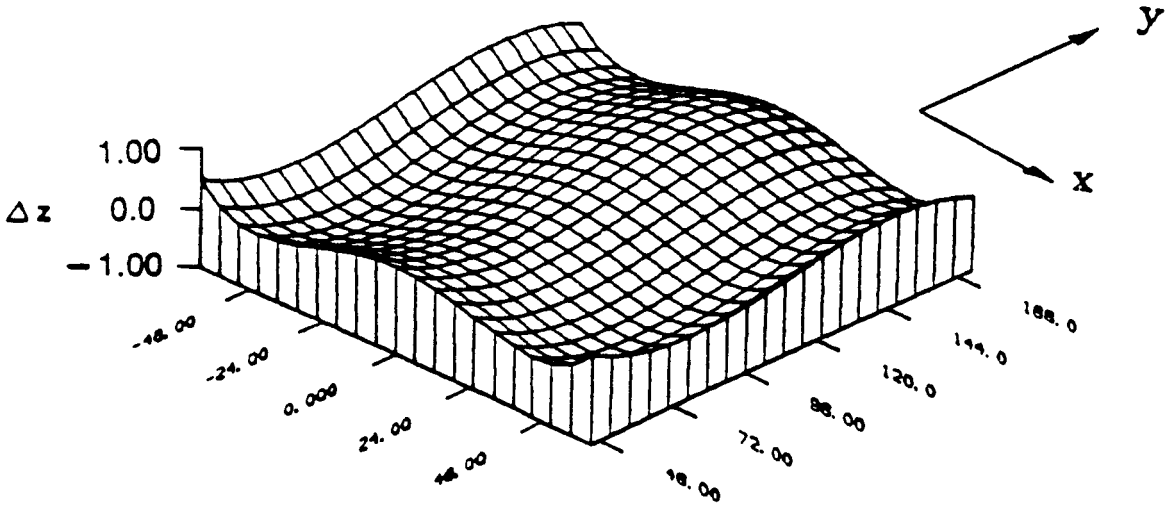

(b) distortion function #2 plotted for $\beta_x = \beta_y = 1\lambda$

FIGURE 6. Distortion Functions Superimposed on the Perfect Parabolic Reflector Sketched in Figure 5.

(Height dimension in wavelengths @ 30 GHz, base dimension in inches)

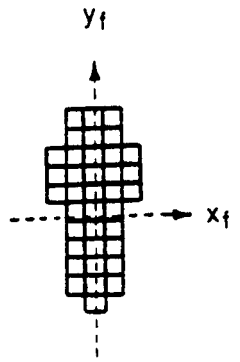

(a) N = 37 Q = 20
D = 1.6 λ A = 95 λ^2

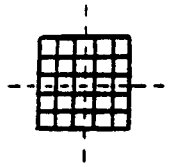

(b) N =25 Q = 20
D = 1.6 λ A = 64 λ^2

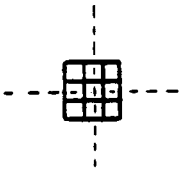

(c) N = 9 Q = 20
D = 1.6 λ A = 23 λ^2

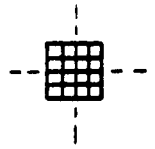

(d) N = 16 Q = 11.25
D = 1.2 λ A = 23 λ^2

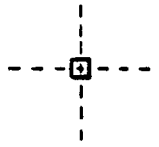

(e) N = 1 Q = 20
D = 1.6 λ A = 2.5 λ^2

Parameter: N = # of elements
D = element spacing
Q = element patern Q (E-plane, and H-plane patterns are given by $\cos^Q\theta$)
A = approximate feed array area

FIGURE 7. Feed Arrays for the Reflector in Figure 5. Each Square Repersents a Feed Element Located at the $z_f = 0$ Plane.

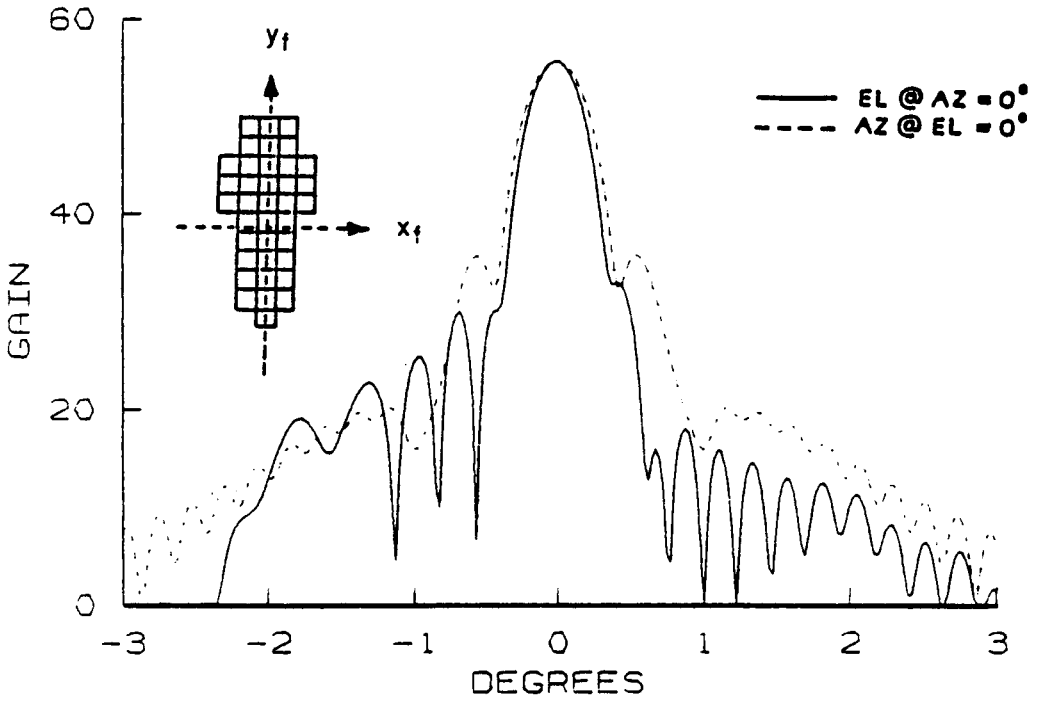

FIGURE 8. Pattern Cuts for the Distorted Reflector with the Array Feed Sketched in Figure 7a.

37 - 38

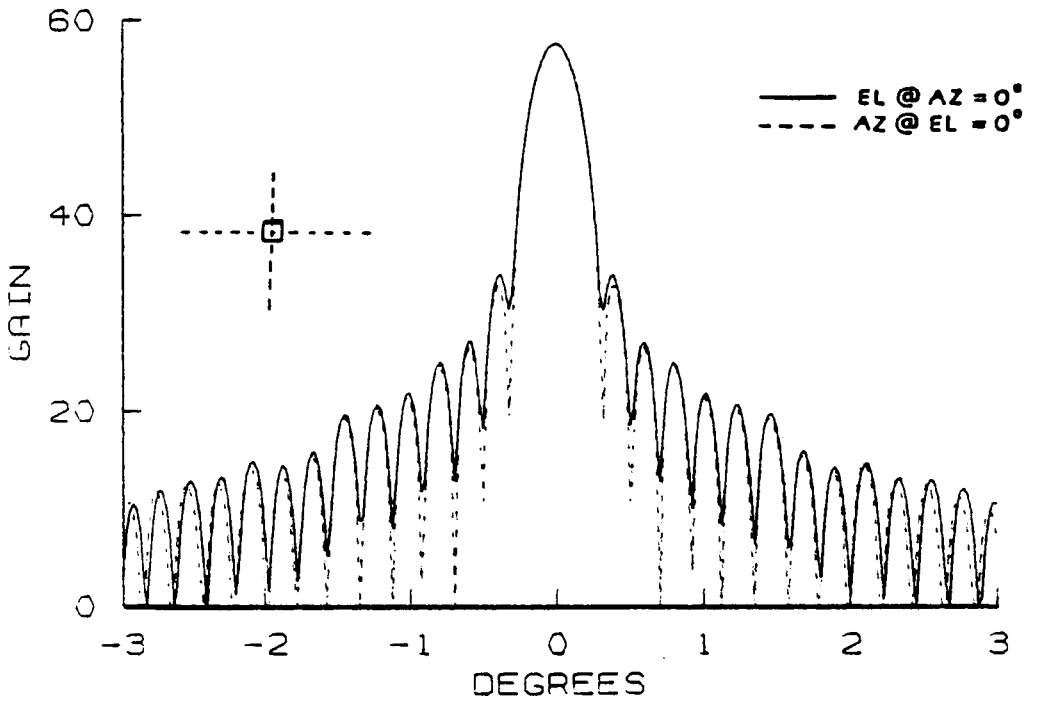

FIGURE 9. Pattern Cuts for the Undistorted Reflector with a Single Feed Element Sketched in Figure 7e.

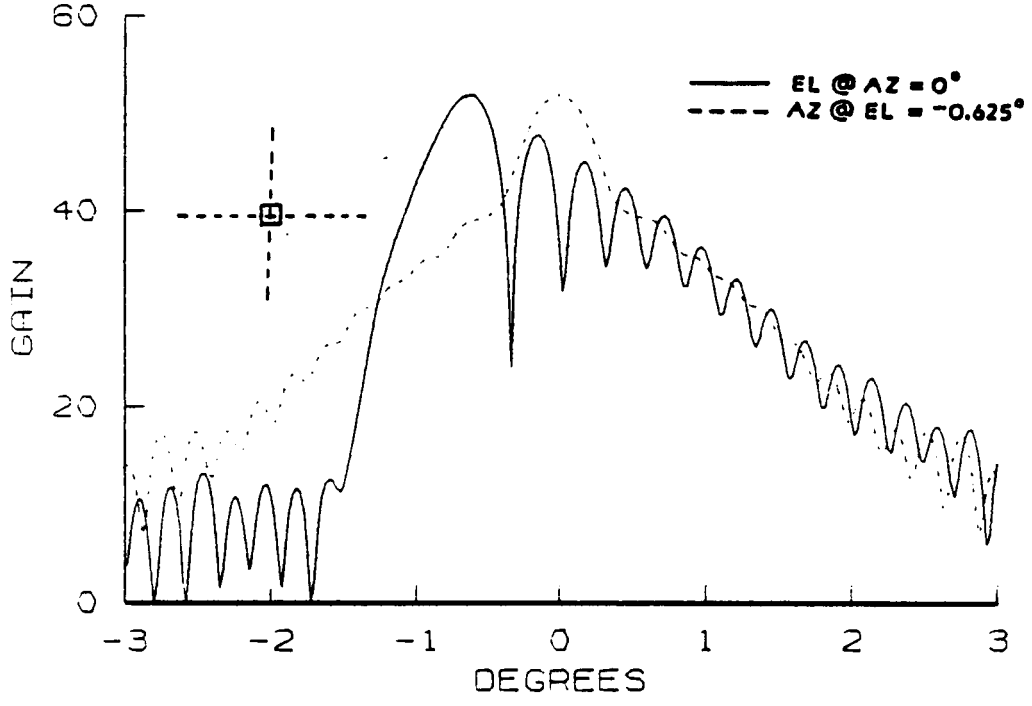

FIGURE 10. Pattern Cuts for the Distorted Reflector with a Single Feed Element Sketched in Figure 7e.

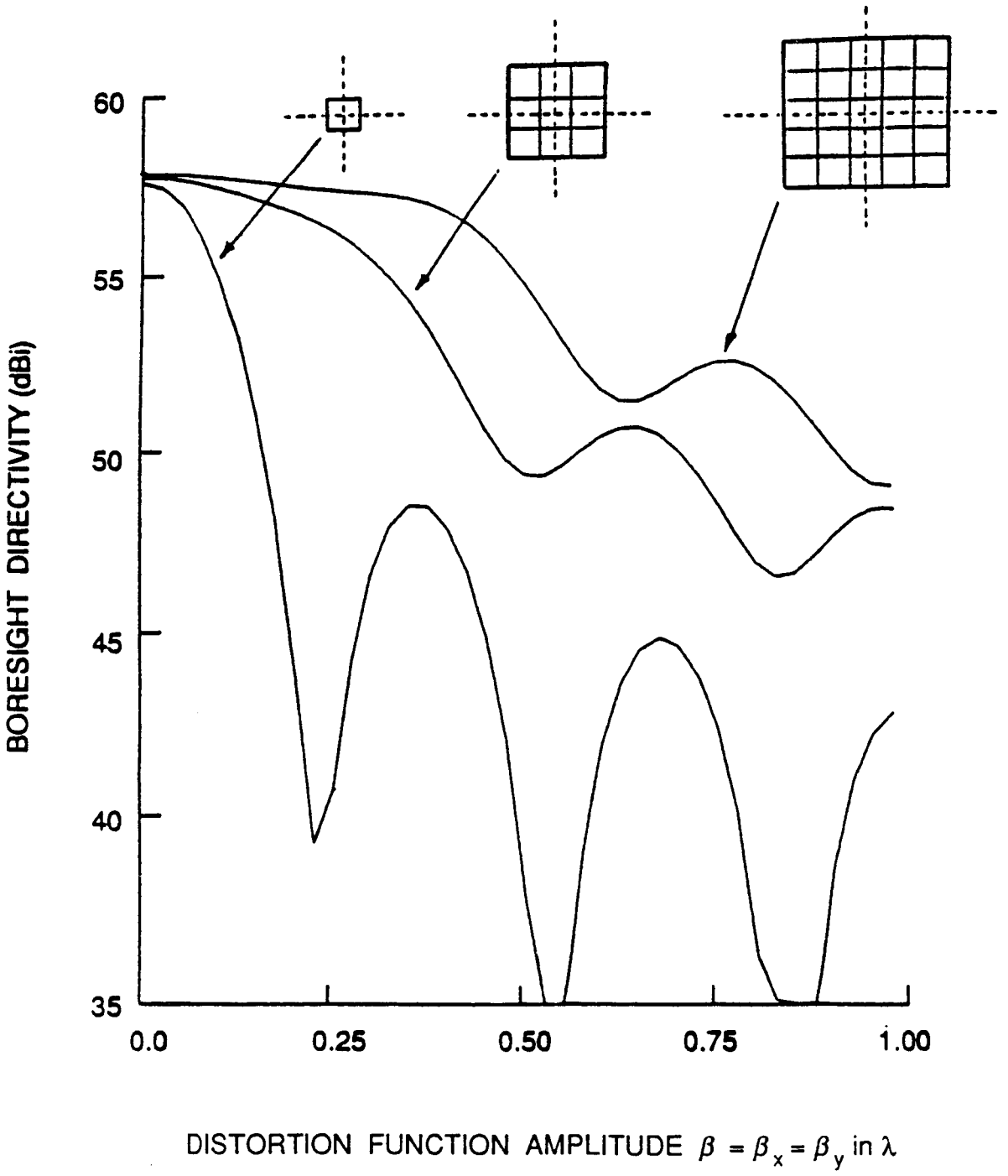

FIGURE 11a. Optimum Boresight Directivity as a Function of Distortion Amplitude for Three Different Array Areas. Distortion function #1 was used when calculating each curve.

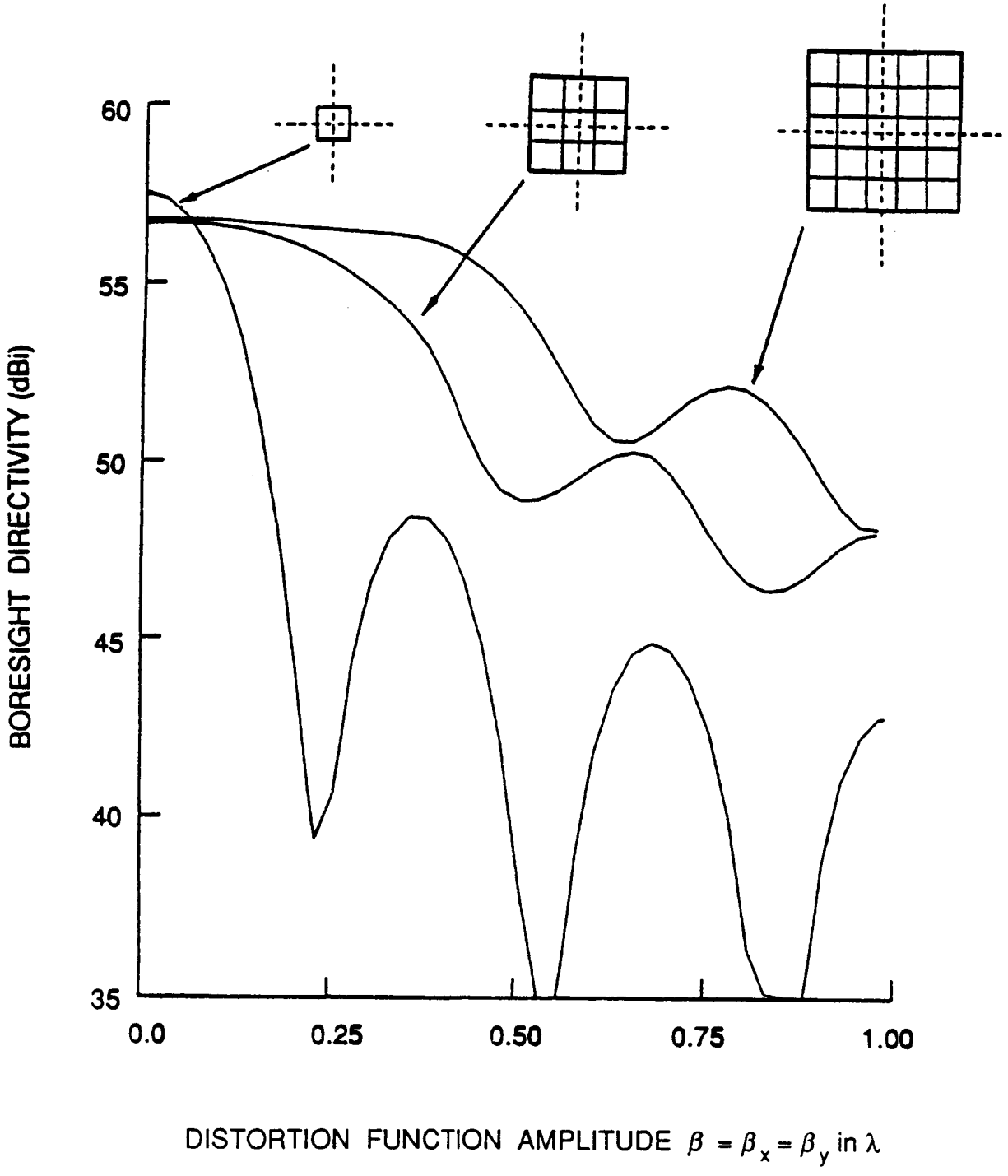

FIGURE 11b. Conjugate Field Matching Boresight Directivity as a Function of Distortion Amplitude for Three Different Array Areas. Distortion function #1 was used when calculating each curve.

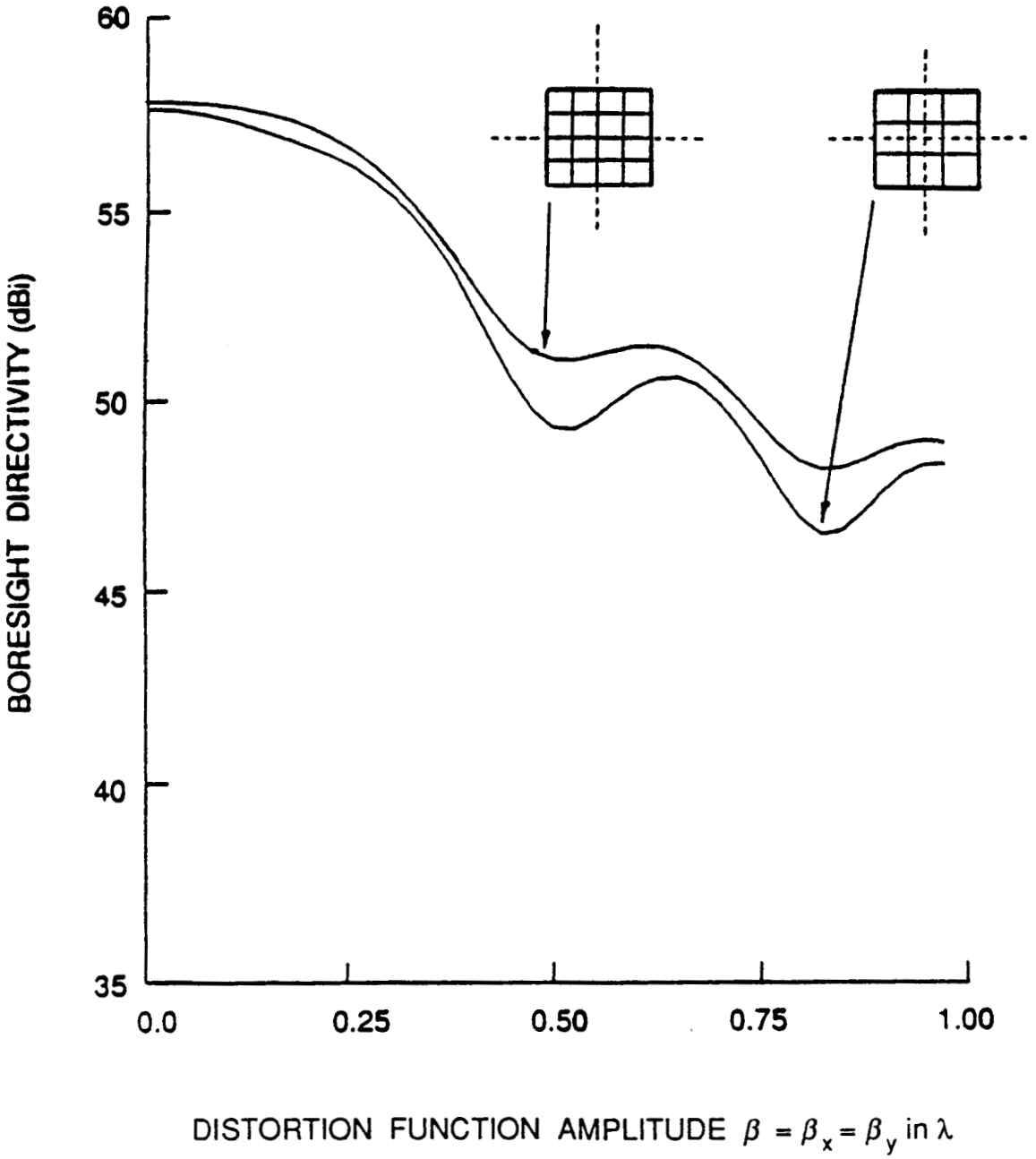

FIGURE 12. Optimum Boresight Directivity as a Function of Distortion Amplitude for Two Different Element Spacings (Equal Array Areas). Distortion function #1 was used when calculating both curves.

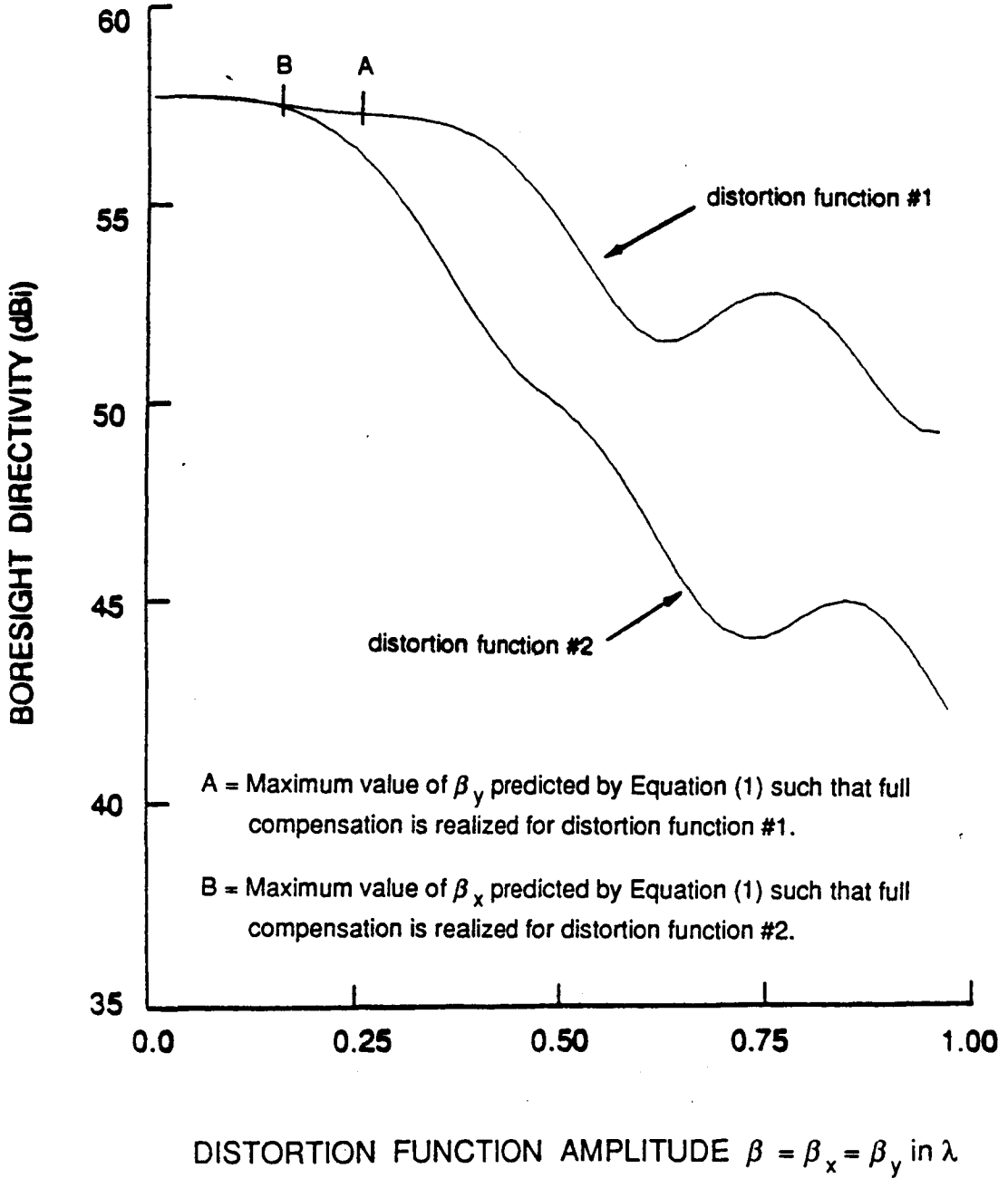

FIGURE 13. Optimum Boresight Directivity as a Function of Distortion Amplitude for Two Different Distortion Functions. The 25 element array of figure 6b was used when calculating both curves.

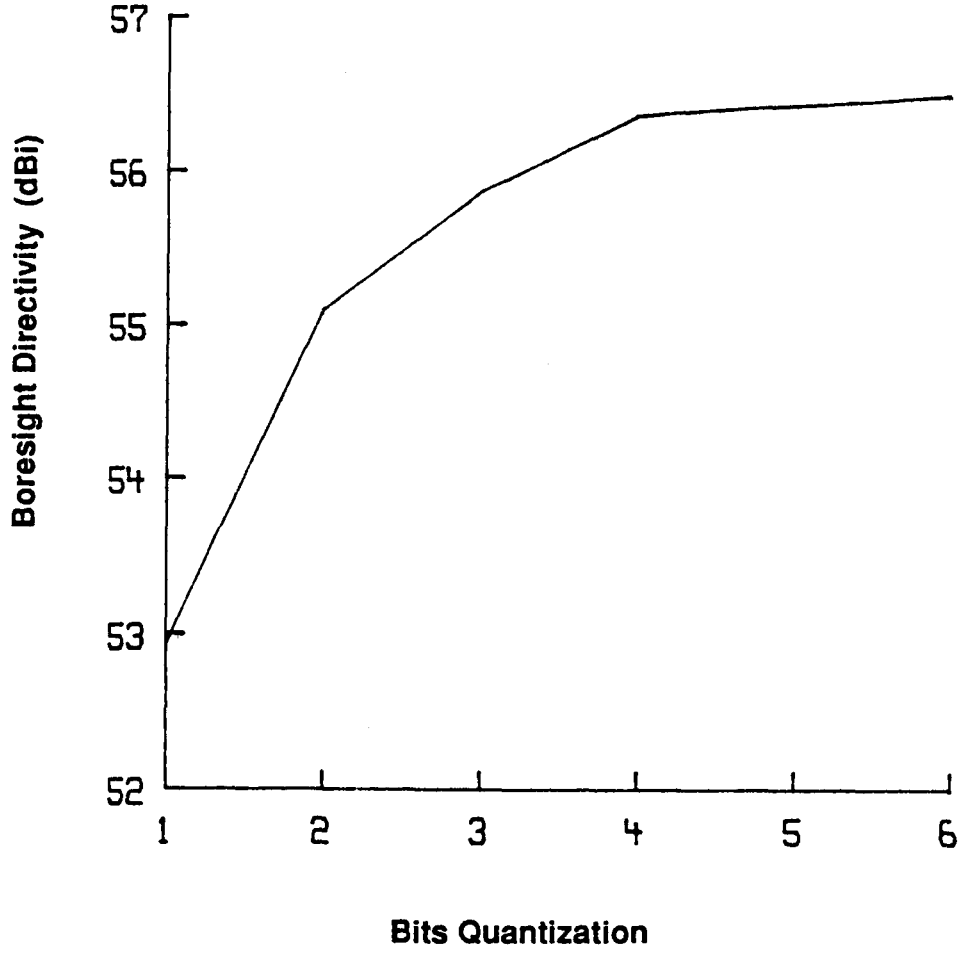

FIGURE 14. Effect of weight quantization on peak boresight directivity. The weights are quantized linearly in phase and amplitude. These results are for the 25 element feed array (Figure 7b) and distortion function #2 ($\beta_x = \beta_y = 0.175\,\lambda$) superimposed on the reflector.

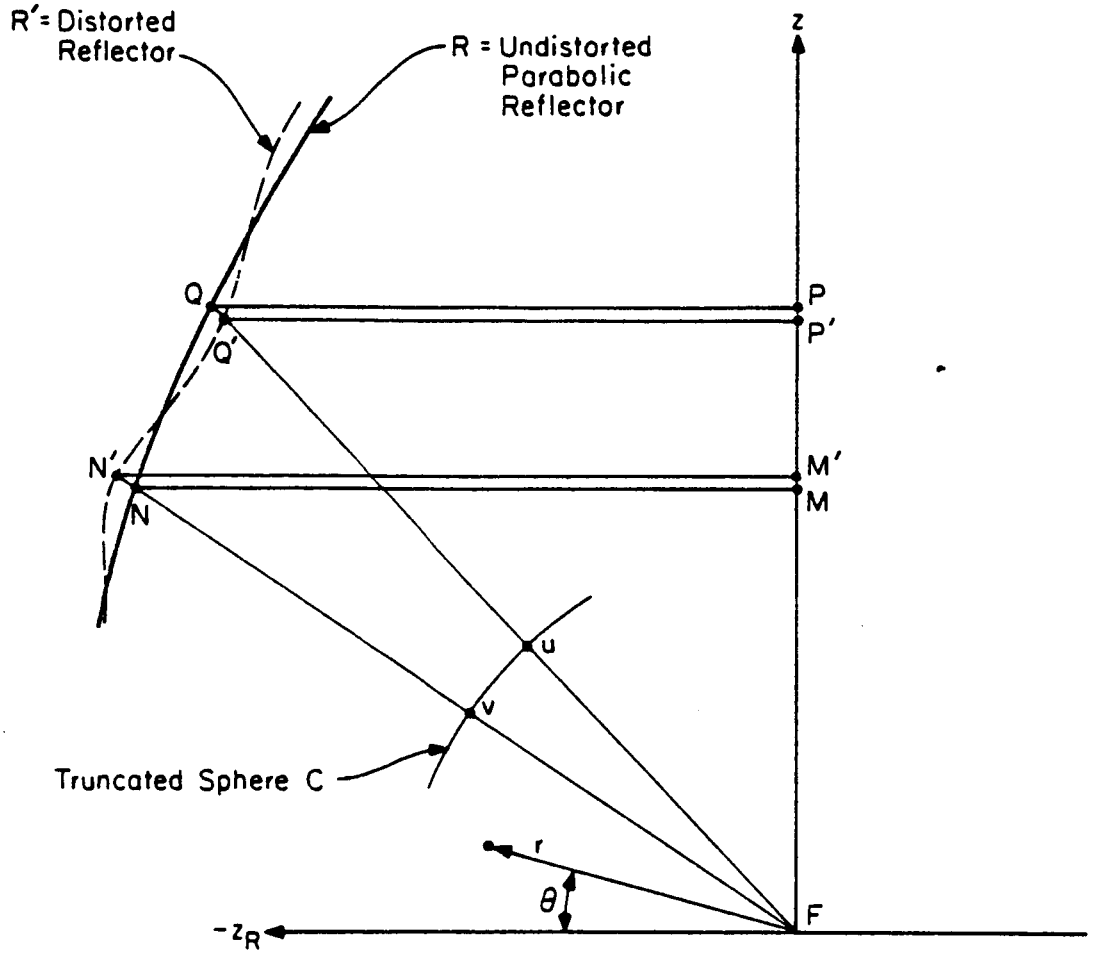

FIGURE 15. Relation Between Surface Distortion and the Resultant Phase Distortion.

NASA
National Aeronautics and Space Administration

Report Documentation Page

1. Report No.	2. Government Accession No.	3. Recipient's Catalog No.
NASA TM-100286		

4. Title and Subtitle	5. Report Date
Compensation of Reflector Antenna Surface Distortion Using an Array Feed	January 1988
	6. Performing Organization Code

7. Author(s)	8. Performing Organization Report No.
A.R. Cherrette, R.J. Acosta, P.T. Lam, and S.W. Lee	E-3929
	10. Work Unit No. 650-60-20

9. Performing Organization Name and Address	11. Contract or Grant No.
National Aeronautics and Space Administration Lewis Research Center Cleveland, Ohio 44135-3191	
	13. Type of Report and Period Covered: Technical Memorandum

12. Sponsoring Agency Name and Address	14. Sponsoring Agency Code
National Aeronautics and Space Administration Washington, D.C. 20546-0001	

15. Supplementary Notes

A.R. Cherrette and S.W. Lee, Unversity of Illinois, Dept. of Electrical and Computer Engineering, Urbana, Illinois 61801 (work performed under NASA Grant NAG3-419); R.J. Acosta, NASA Lewis Research Center; P.T. Lam, Lockheed Missiles and Space Company, Sunnyvale, California 94088.

16. Abstract

The dimensional stability of the surface of a large reflector antenna is important when high gain/low sidelobe performance is desired. If the surface is distorted due to thermal or structural reasons, antenna performance can be improved through the use of an array feed. The design of the array feed and its relation to the surface distortion are examined in this paper. The sensitivity of antenna performance to changing surface parameters for fixed feed array geometries is also studied. This allows determination of the limits of usefulness for feed array compensation.

17. Key Words (Suggested by Author(s))	18. Distribution Statement
Compensation; Reflector antenna; Surface distortion; Numerical analysis; Electromagnetic fields	Unclassified - Unlimited Subject Category 32

19. Security Classif. (of this report)	20. Security Classif. (of this page)	21. No of pages	22. Price*
Unclassified	Unclassified	48	A03

NASA FORM 1626 OCT 86

*For sale by the National Technical Information Service, Springfield, Virginia 22161